

Annual cycle of equatorial zonal currents in the Pacific

Noel Keenlyside¹

Department of Mathematics and Statistics, Monash University, Clayton, Victoria, Australia

Richard Kleeman

Courant Institute for Mathematical Sciences, New York University, New York, USA

Received 7 November 2000; revised 26 November 2001; accepted 10 December 2001; published 3 August 2002.

[1] Observational (Tropical Atmosphere-Ocean array) data on the annual cycle of upper ocean zonal currents on the equator are analyzed using a simple dynamical ocean model in order to investigate underlying dynamics. The model, by treating linear and nonlinear terms semi-independently, allows a separation of various linear and nonlinear effects. The model focuses on linear dynamics of low-order baroclinic modes. By realistically simulating the vertical structure of annual cycle, the model shows that linear dynamics determines the vertical and meridional structure of the annual cycle. Nonlinearity is weak and only important in the undercurrent, where it provides a simple mechanism for the annual cycle: mean meridional advection of the annual cycle north of the equator onto the equator, with the boreal springtime surge in the undercurrent being a direct result of a surge centered at 2°N. Model results show that annual variations in zonal currents are out of phase across the equator, surging in the corresponding spring. This behavior is a response to trade wind variations, which are also equatorially antisymmetric, and is generated by the second meridional mode Rossby wave. *INDEX TERMS*: 4231 Oceanography: General: Equatorial oceanography; 4255 Oceanography: General: Numerical modeling; 4512 Oceanography: Physical: Currents; *KEYWORDS*: tropical Pacific, equatorial ocean currents, zonal momentum balance, baroclinic mode model, equatorial waves, equatorial undercurrent

1. Introduction

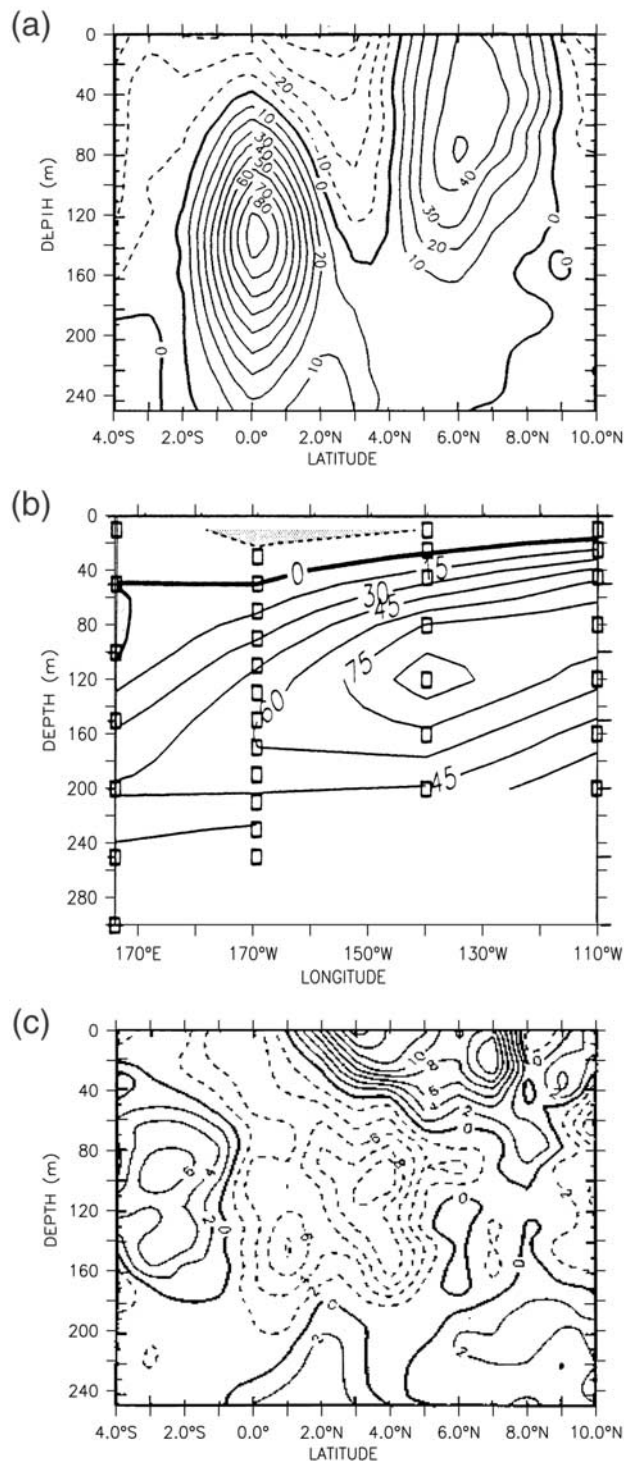
[2] Understanding the dynamics of the equatorial Pacific is important to world climate. The climate's sensitivity to sea surface temperature in this region is well accepted. On interannual timescales the strong air-sea interaction is a dominant driving force for the El Niño Southern Oscillation [Philander, 1990]. On longer timescales the role of the air-sea interaction and how it may change under global warming scenarios is not well understood and is an active area of research. The equatorial undercurrent (EUC), a strong eastward subsurface jet, transports water into a region where the air-sea interaction is important. As much of this water originates in the extratropics [McCreary and Lu, 1994; Johnson and McPhaden, 1999], the EUC may play an important role in both decadal variability [Gu and Philander, 1997] and in determining the climate's response to global warming [Cai and Whetton, 2000]. Together with the necessary reliance of climate and climate change studies on complex models, it is important to understand and accurately model the dynamics of the EUC.

[3] In the past, currents have not contributed significantly to model testing and mechanism analysis because of the limited amount of data. Now, though, measurements

from several moored buoys in the Pacific are providing sufficient data to give an accurate picture of the annual cycle of zonal currents along the equator, over the upper 200 m (Tropical Ocean-Global Atmosphere (TOGA) experiment Tropical Atmosphere-Ocean (TAO) array [Yu and McPhaden, 1999b]). The annual cycle is characterized by an eastward surge, which extends from the surface to the core of the EUC, that occurs around April–July when the trade winds are weak. At the surface the surge is strong enough to cause the reversal of the westward south equatorial current (SEC). The observational and modeling work of Yu and McPhaden [1999a, 1999b] explains the surge at the surface as due to the unbalanced eastward pressure gradient that occurs when the winds are weak. The zonal structure of the surge is determined by linear wave dynamics.

[4] The penetration of the eastward surge into the EUC is not easily understood. For one, it is well accepted that the trade winds drive the EUC, not directly but through the eastward pressure gradient they create [Philander, 1990]. Second, observational [Johnson and Luther, 1994; Qiao and Weisberg, 1997] and modeling studies [Wacongne, 1989] both indicate that wind stress is not important in the momentum balance of the EUC. Third, observational work on the parameterization of vertical mixing [Peters et al., 1988] shows that short-term wind stress variability does not penetrate to the EUC core. All these suggest that the slackening of the winds could only indirectly effect the annual cycle of the EUC, either through nonlinearity or by

¹Also at Max Planck Institute for Meteorology, Hamburg, Germany.



altering the pressure gradient; however, any relaxation in the gradient of the thermocline (caused by the slackening of the winds) would weaken rather than strengthen the EUC.

[5] Nonlinear models are able to realistically reproduce the annual cycle of the EUC [Yu *et al.*, 1997]. Similar studies with linear models do not exist. In this paper a simple model is used to systematically decompose the observations of zonal currents along the equator into linear and nonlinear effects, focusing on the annual cycle of the EUC. The results presented here indicate that the annual cycle of the EUC is

not a linear effect but is set up by weak nonlinearity due to mean advection by the meridional circulation.

[6] The remainder of the paper is as follows. In section 2, observations are used to describe the mean and annual cycle of equatorial currents in the Pacific. Section 3 describes the model used, explaining how it permits a separate analysis of linear and nonlinear effects. In section 4, the model's simulation of the mean and annual cycle are presented, with linear and nonlinear contributions described. In section 5, a detailed analysis is given to explain the underlying mechanism for the annual cycle of the EUC. This is followed by a summary in section 6. Last, the full model equations are given in Appendix A, and model sensitivity studies are summarized in Appendix B.

2. Observational Description of the Equatorial Currents

[7] In this section, observations are used to describe the mean equatorial circulation and the annual cycle of the zonal currents. Profiling current meter data from the North Pacific Experiment (NORPAX) Hawaii-to-Tahiti Shuttle [Johnson and Luther, 1994] and moored current meter data from the TAO buoy array [Yu and McPhaden, 1999a, 1999b] are both used. The meridional structure of the zonal and meridional mean currents around 150°–160°W is revealed by the NORPAX data (Figures 1a and 1c), as discussed by Johnson and Luther [1994]. The TAO buoy data allow a description of the zonal structure and annual cycle of zonal currents along the equator in the upper 250–300 m [Yu and McPhaden, 1999a, 1999b].

2.1. Observational Mean

[8] Equatorial zonal currents (Figures 1a and 1b) consist of a weak westward surface current, the SEC, and an intense subsurface eastward current, the EUC. To the north the eastward flowing north equatorial counter current (NECC) is also seen (centered at 6°N in Figure 1a). The EUC is centered on the equator and is strongly equatorial-trapped. In the central Pacific it is 200 m thick and 300 km wide (and centered at 120 m in Figure 1a). The core of the EUC rises from 180 m at 180°E to 80 m at 110°W and is strongest in the central eastern Pacific, where it averages speeds $>0.9 \text{ m s}^{-1}$ (Figure 1b). The SEC is directly above the EUC; it is significantly weaker and shoals toward the east.

Figure 1. (opposite) Observations of the annual mean structure of zonal and meridional currents. (a) The meridional structure of zonal currents in the eastern central Pacific, (b) the zonal structure of zonal currents along the equator, and (c) the meridional structure of meridional currents in the eastern central Pacific. Units are cm s^{-1} , solid lines indicate positive flow, and dashed lines indicate negative flow. Figures 1a and 1c are taken from Johnson and Luther [1994] and were constructed using data between 160° and 150°W from the Hawaii-to-Tahiti shuttle experiment. Figure 1b is taken from Yu and McPhaden [1999a] (reprinted with permission from the American Meteorological Society) and is constructed using data from the Tropical Ocean-Global Atmosphere (TOGA) experiment Tropical Atmosphere-Ocean (TAO) array; boxes indicate measurement positions.

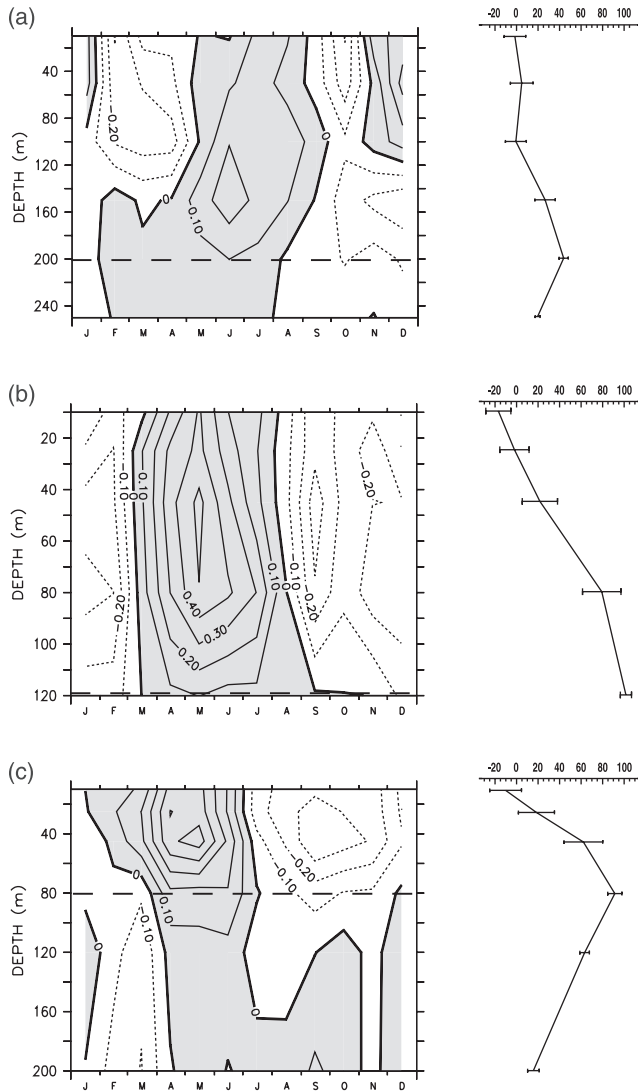


Figure 2. The annual cycle of zonal currents at (a) 165°E , (b) 140°W , and (c) 110°W calculated from TAO data; the data are detailed by Yu and McPhaden [1999a, 1999b]. The left-hand side shows the annual cycle of zonal currents in terms of velocity anomalies (m s^{-1}). Dashed horizontal lines mark the depth of the undercurrent core on each plot. The right-hand side shows the annual mean vertical structure of zonal currents (cm s^{-1}) at the three locations. Horizontal bars indicate 95% confidence interval calculated using the Student's *t*-distribution. The position of the bars also corresponds to measurement depths. Note that owing to missing data the vertical scales among plots differ.

[9] The meridional currents (Figure 1c) are significantly weaker than the zonal currents. The flow, which at the surface is divergent about the equator and at the level of the undercurrent is convergent, can be characterized as two overturning cells with upwelling along the equator. This feature, which is seen in other data of the central and eastern Pacific, shall be referred to as the equatorial cell.

2.2. Observational Annual Cycle

[10] TAO data are now used to describe the annual cycle of zonal currents on the equator at 165°E , 140°W , and

110°W (Figure 2). The data have been used previously to describe the annual cycle of these currents [Yu and McPhaden, 1999a, 1999b]. This description differs by focusing on the annual cycle of the EUC rather than the vertically averaged currents.

[11] Following Yu and McPhaden [1999a], the annual cycle is described in terms of velocity anomalies (i.e., variations about the mean). The mean vertical structure is indicated on the left-hand side of Figure 2. Additionally, the depth of the EUC is marked on the velocity anomaly plots with a horizontal dashed line. The vertical scale differs among the plots (since only Mechanical Current Meter data available for longer than 7 years are used), but at all locations, data extend to the depth of the EUC.

[12] The annual cycles at all three locations have very similar structures. There is an eastward surge in the currents, occurring between April and July, which extends from the surface to the depth of the undercurrent. The phase of the surge is fairly depth-independent and has its largest amplitude 60 m above the EUC core. This surge, occurring in the northern spring, shall be referred to as the springtime surge (STS).

[13] Comparing the mean structure with the annual cycle shows that the eastward STS is strong enough to cause an eastward current at the surface. This is known as the springtime reversal of the SEC. The phase of the reversal propagates westward and has been documented in the literature [Yu and McPhaden, 1999a]. Westward phase propagation is also evident with depth, but the phase speed decreases, being close to zero at the depth of the EUC.

[14] Figure 2 shows that the annual cycle of the undercurrent, including the STS, is weak relative to the annual cycle above the undercurrent. In Figure 3 the annual cycle of the EUC is illustrated more clearly. At all locations, annual variations are between 10% and 20% of the mean. Error bars show that the eastward surge is significant but westward phase propagation is not; the surge occurs at all locations around April–May.

[15] Although the EUC is probably tied to the thermocline, which has a weak annual cycle [Yu and McPhaden, 1999a], annual variations in the depth of the EUC core are ignored (in Figure 3 and later analysis). Observations are not adequate to resolve the latter; however, the levels chosen always remain within the EUC core.

3. Dynamical Ocean Model

[16] In the remainder of the paper the annual cycle of zonal currents will be analyzed to determine the importance of linear and nonlinear terms and to explain the basic mechanisms. The main tool is a simple dynamical ocean model, which consists of a linear and a nonlinear component. The linear component is basically a *McCreary* [1981] type modal model, but it is extended to have a horizontally varying background stratification. It is the dominant component, largely determining the structure and magnitude of the solution. The nonlinear component is a highly simplified model of the residual nonlinear momentum equations. It provides important corrections to the solution where the linear assumption breaks down. A summary of

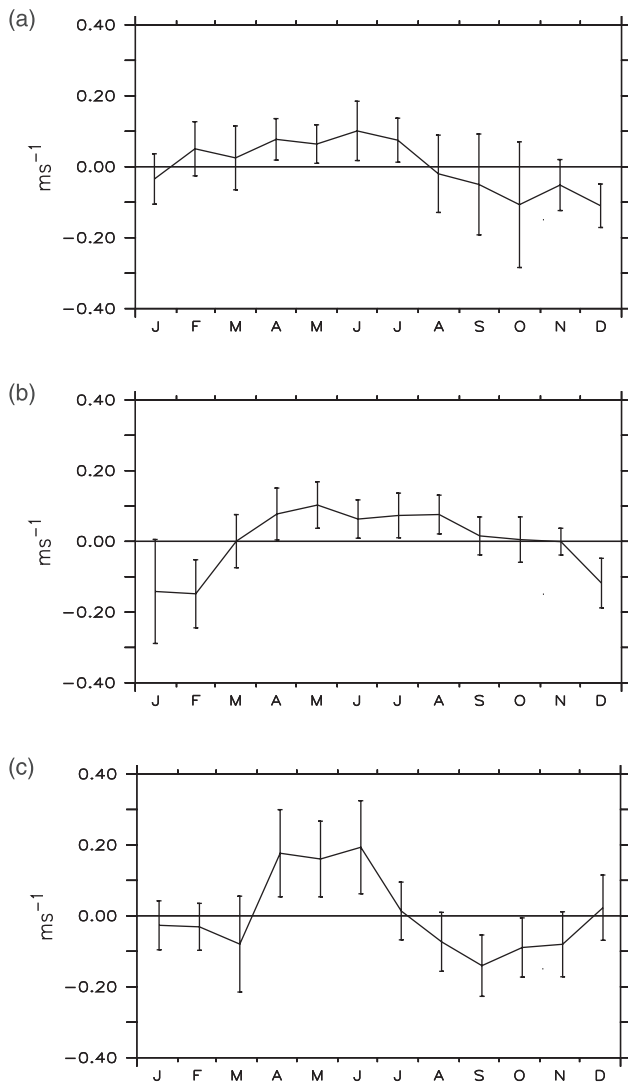


Figure 3. The annual cycle of zonal velocity anomaly (m s^{-1}) at (a) 165°E , 0°N at 200 m; (b) 140°W , 0°N at 120 m; (c) 110°W , 0°N at 80 m. The depth at each location corresponds to the depth of the equatorial undercurrent (EUC) core; hence these plots illustrate the annual cycle of the EUC. Vertical bars indicate the 90% confidence interval calculated from the interannual variability of the data using a Student's *t*-distribution. The data are from the TOGA TAO array and are detailed by *Yu and McPhaden* [1999a, 1999b].

the model's important features will now be given; the full set of equations are given in Appendix A.

[17] The model's design is motivated as follows. First, a large amount of observational evidence and experimental results exist that show that linear dynamics, generally associated only with the low-order baroclinic modes, can successfully explain many features of the equatorial Pacific ocean [*McCreary*, 1981; *Yu and McPhaden*, 1999a, 1999b; *Cane*, 1984]. Second, there are regions where nonlinearity is important, for example, in the momentum balance of surface zonal currents [*Wacongne*, 1989] and the annual cycle of the EUC (to be shown in section 4.2). Third, horizontal variations in stratification

are important, having a significant effect on the wind projection onto baroclinic modes and hence the solution [*Dewitte et al.*, 1999].

[18] The linear component consists of a 10 baroclinic mode model plus two surface layers, which are governed by Ekman dynamics and represent a simplified treatment of baroclinic modes 11–30 (see Appendix A). A 10 mode solution insures that all fields are converged [*Minobe and Takeuchi*, 1995], and a contribution for modes 11–30 is included because of their role in the meridional circulation. In Appendix A it is shown that high-order modes, being strongly damped, are consistently approximated by Ekman dynamics. The baroclinic modes, which vary horizontally, are calculated from *Levitus's* [1982] mean temperature and salinity data. Baroclinic modes were also calculated using *Levitus* monthly mean data, but model results were not greatly sensitive. The shallow water speeds associated with the modes, taken as horizontally constant, are obtained from 180°E , 0°N . Table 1 lists the shallow water speeds for the first 10 modes.

[19] The linear component is a solution to the following equations, which are almost identical to *McCreary's* [1981]:

$$\begin{aligned}
 u_t - f_v &= -p_x + \nu_h \nabla_h^2 u + (\nu_v u_z)_z \\
 v_t + fu &= -p_y + \nu_h \nabla_h^2 v + (\nu_v u_z)_z \\
 p_z + \rho g &= 0 \\
 \nabla \cdot \mathbf{u} &= 0 \\
 \rho_t - \frac{w}{g} N^2 &= \kappa_h \nabla_h^2 \rho + (\kappa_v \rho)_{zz}
 \end{aligned} \tag{1}$$

where surface boundary conditions are $\nu_v u_z = \tau^x$, $\nu_v v_z = \tau^y$, $\kappa_v \rho = 0$, and $w = \eta$; bottom boundary conditions are $\nu_v u_z = \nu_v v_z = \kappa_v \rho = w = 0$; and there is no slip at lateral boundaries. Here u , v , and w are the velocities in the east, west, and vertical downward directions, respectively; $p (= \frac{p}{\rho_0})$ is the kinematic pressure; $\rho (= \frac{\rho}{\rho_0})$ is the specific gravity where ρ_0 is the mean ocean density; $N^2 = -g\rho_0^{-1} \bar{\rho}_z$ is the background Brunt-Väisälä frequency; g is gravity; $\bar{\rho}(x, y, z)$ is the mean density; ∇_h is the horizontal divergence operator; f is the Coriolis parameter; ν_h and ν_v are the horizontal and vertical eddy diffusivities for momentum; κ_h and κ_v are the horizontal and vertical eddy diffusivities for heat; τ^x and τ^y are the zonal and meridional surface wind stress; and η is the free surface.

Table 1. Shallow Water Speeds for the Model's First 10 Baroclinic Modes^a

Baroclinic Mode	Shallow Water Speed
1	2.96
2	1.84
3	1.13
4	0.82
5	0.66
6	0.57
7	0.47
8	0.41
9	0.38
10	0.35

^a Speeds were calculated using stratification at 180°E , 0°N and are given in $\text{C} (\text{m s}^{-1})$ [*Levitus*, 1982].

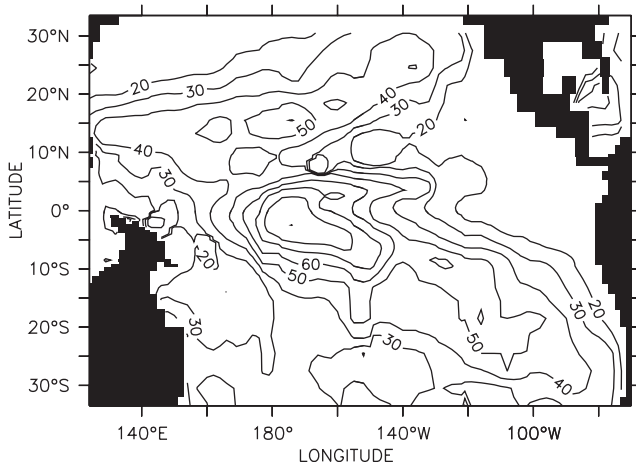


Figure 4. The model's mixed layer depth, calculated from *Levitus's* [1982] data as described in the text, contoured with an interval of 10 m. The model's land-sea mask is also shown as shaded areas.

[20] The equations in (1) primarily differ from *McCreary's* [1981] in that N^2 varies horizontally. They are obtained as a linearization of the equations of motion about a resting state, neglecting horizontal density gradients in the density equations. This step, standard in linear models, assumes that density-driven currents are negligible. While this assumption is dubious at best, it still allows good results. Our modal solution is obtained as follows. First, following *McCreary*, take the vertical coefficients for diffusivity of momentum and heat to be inversely proportional to the Brunt-Väisälä frequency squared and to be identical (i.e., $\nu_v = \kappa = \frac{A}{N^2}$, where A is referred to as the vertical diffusion parameter). Second, neglect mode mixing due to horizontal varying background stratification. Sensitivity experiments indicate that both of these assumptions are reasonable (Appendix A). Our solution primarily differs from *McCreary's* by using the local modes (i.e., calculated from the local vertical structure). This allows spatially varying wind projection coefficients and gives the solution a much more realistic vertical and zonal current structure (see Figure 5).

[21] The nonlinear component satisfies the following equations:

$$\begin{aligned} u_t^{nl} + \mathbf{u} \cdot \nabla(u) &= \nu_h \nabla_h^2(u^{nl}) + (\nu_v u_z^{nl})_z, \\ \nabla \cdot \mathbf{u}^{nl} &= 0, \end{aligned} \quad (2)$$

but is only solved within two surface layers identical to those used to simulate high-order baroclinic modes. The residual zonal velocity is \mathbf{u}^{nl} , and $\mathbf{u} = \mathbf{u}^l + \mathbf{u}^{nl}$ is the total zonal velocity, with \mathbf{u}^l being the contribution from the linear component. These equations are obtained directly from the residual nonlinear momentum equations and boundary conditions, assuming that ρ^{nl} , p^{nl} , and v^{nl} can be neglected. By definition the residual equations describe the terms neglected in linearizing. Hence these equations are forced through the nonlinear advective terms not via boundary conditions but by the linear equations. Scale analysis justifies neglect of v^{nl} . As stated above, the

neglect of ρ^{nl} and p^{nl} is less straightforward but is assumed, and given the model's performance, it does not seem a major concern. The nonlinear component is highly simplified, designed only to capture the dominant nonlinearity and its effect on the EUC, SEC, and the meridional circulation. Being simplified, it is better able to illustrate dominant mechanisms.

3.1. Implementation

[22] The model spans the Pacific and Atlantic oceans. (Only results from the Pacific basin are included here.) Its domain extends from 124°W–30°E and from 33.5°S–33.5°N. An Arakawa c-grid is used with 2° zonal grid spacing and a stretched meridional grid, with 0.5° grid spacing within 10° of the equator, extending to 3° at the boundaries. A realistic representation of land is also included (see Figure 4).

[23] Vertically, a 5500 m flat-bottomed ocean is assumed. The vertical grid of the linear component has 33 levels. The grid spacing, with 8 levels in the surface 125 m, focuses on resolving surface dynamics. The 2 layers used to simulate nonlinear effects and high-order baroclinic modes cover the upper 125 m and are divided by the mixed layer depth. The mixed layer is defined on a stability criterion, effectively, as surface water with $N^2 < 6.5 \times 10^{-6} \text{ s}^{-2}$. The model's mixed layer (Figure 4) was calculated from *Levitus's* [1982] mean temperature and salinity data.

[24] The coefficients for horizontal diffusion of heat and momentum are assumed to be equal and are identical for both the linear and nonlinear components. The coefficient in the zonal direction is $2.5 \times 10^4 \text{ m}^2 \text{ s}^{-1}$. In the meridional direction the coefficient is $2.5 \times 10^3 \text{ m}^2 \text{ s}^{-1}$ in the interior but increases linearly over the outer seven grid points to a value of $1.275 \times 10^5 \text{ m}^2 \text{ s}^{-1}$. The vertical diffusion parameter is taken as $1 \times 10^{-7} \text{ m}^2 \text{ s}^{-3}$, which gives equivalent values for the coefficient of vertical diffusion of $(6-4) \times 10^{-2} \text{ m}^2 \text{ s}^{-1}$ in the mixed layer and $3 \times 10^{-4} \text{ m}^2 \text{ s}^{-1}$ in the EUC core and was chosen to match surface observation by *Peters et al.* [1988] of $(3-6) \times 10^{-2} \text{ m}^2 \text{ s}^{-1}$. The coefficient of vertical diffusion in the nonlinear model is $1 \times 10^{-3} \text{ m}^2 \text{ s}^{-1}$. Sensitivity studies indicate that these parameter values are appropriate (Appendix A).

4. Results

[25] The mean and annual cycles discussed in this section are obtained from the final year of a 10 year model run and are forced from rest with the *Hellerman and Rosenstein* [1983] climatological wind stress and reduced in magnitude by 20% [*Harrison, 1989*]. The model is almost spun up after 3 years and by 10 years the annual cycle shows no year-to-year variations. The model's sensitivity to wind stress is covered in Appendix A.

4.1. Modeled Mean

[26] The model is able to realistically capture the large-scale features of the equatorial circulation both in terms of magnitude and structure (Figure 5). The depth and eastward rise of the EUC are realistic (Figure 5b). It is a little stronger than the observations and too confined vertically, but its meridional structure is quite accurate (Figure 5a). The magnitude and width of the SEC

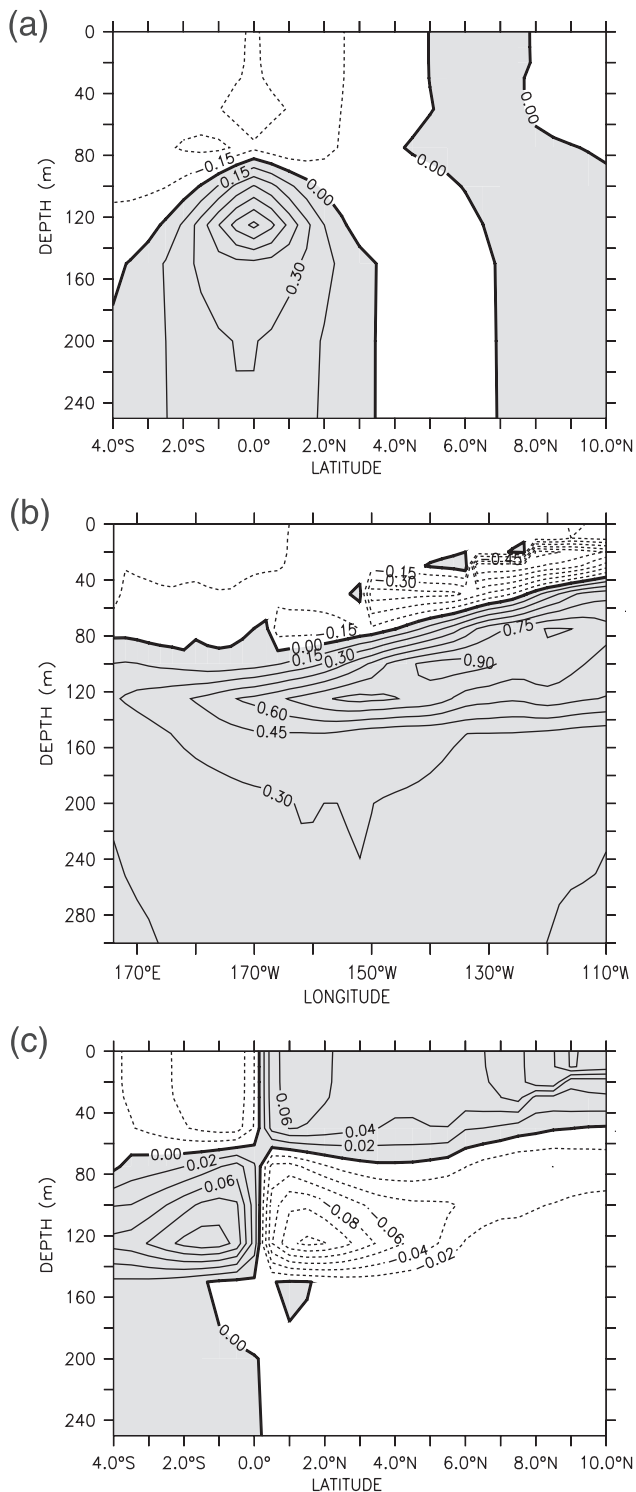


Figure 5. The annual mean structure of the model's zonal and meridional currents. (a) The meridional structure of zonal currents at 154°W , (b) the zonal structure of zonal currents along the equator, and (c) the meridional structure of meridional currents at 154°W . Units are m s^{-1} ; the contour interval for zonal currents is 0.15 m s^{-1} and for meridional currents is 0.02 m s^{-1} . Shading shows eastward and northward flow. (Figure 5 may be directly compared with the observations presented in Figure 1.)

compares well to observations, but it is too deep. Discontinuity above the EUC, most apparent in Figure 5b, is due to the differing resolutions of linear and nonlinear models. The NECC is well positioned but much weaker than observed. *Yu et al.* [2000] have attributed this problem, which is common to many models, to be due to inaccuracies in the wind field.

[27] Consistent with *McCreary* [1981], the magnitude of the EUC and its vertical, meridional, and zonal structures are due to the linear component. Nonlinearity, primarily vertical advection of zonal momentum, is important for maintaining the realistic magnitude of the SEC. This is consistent with both observational [*Johnson and Luther, 1994*] and modeling studies [*Wacongne, 1989*]. Being represented by only two layers, nonlinearity, though working correctly, only effects the magnitude of the currents. As a result, the EUC is not vertically stretched, and the SEC is too deep.

[28] The model's meridional circulation between 160°E and 100°W consists of a well-defined equatorial cell centered roughly about the equator. Consistent with subsurface flow being geostrophic, the subsurface branch is weak outside of this region, since the zonal pressure gradient is small there. The model's meridional circulation at 152°W (Figure 5c) has realistic magnitude and appropriate structure (Figure 1c), but the cross-equatorial southward flow, seen in the observations, that extends from the surface down to 160 m is not present. Direct estimates of meridional velocity [*Johnson and Luther, 1994*; *Qiao and Weisberg, 1997*; *Johnson et al., 2001*] and TAO data used here [*Yu and McPhaden, 1999a, 1999b*] all indicate an equatorial cell. However, tropical instability waves and interannual variability make observational evaluation of its detailed structure difficult. It is thus not possible with available data to assess how well the model simulates the equatorial cell. Overall, the results in this section indicate that the model is able to capture the mean state well, and nonlinearity is working correctly.

4.2. Modeled Annual Cycle

[29] The model annual cycle of equatorial zonal currents (Figure 6) matches the observations (Figure 2) well. The STS is present at all three locations and has a realistic magnitude and phase, but toward the east it becomes surface-trapped.

[30] Decomposition of the results into linear and nonlinear components shows the following. At 165°E , linear dynamics accurately models the annual cycle. The nonlinear component degrades the solution, strengthening it but having little effect on the phase. Similarly, at 140°W and 110°W in the surface layer, linear dynamics accurately models the annual cycle, and the addition of nonlinearity degrades the solution by significantly weakening the annual cycle. In the EUC the situation is quite different. At 140°W , certain aspects of the annual cycle are well modeled, in particular the STS, but here the linear component, hence linear dynamics, cannot simulate the annual cycle. It is the nonlinear component that is responsible for the correct features (Figure 7).

[31] Perhaps the greatest insight into the annual cycle of the EUC is given by the meridional structure (about the

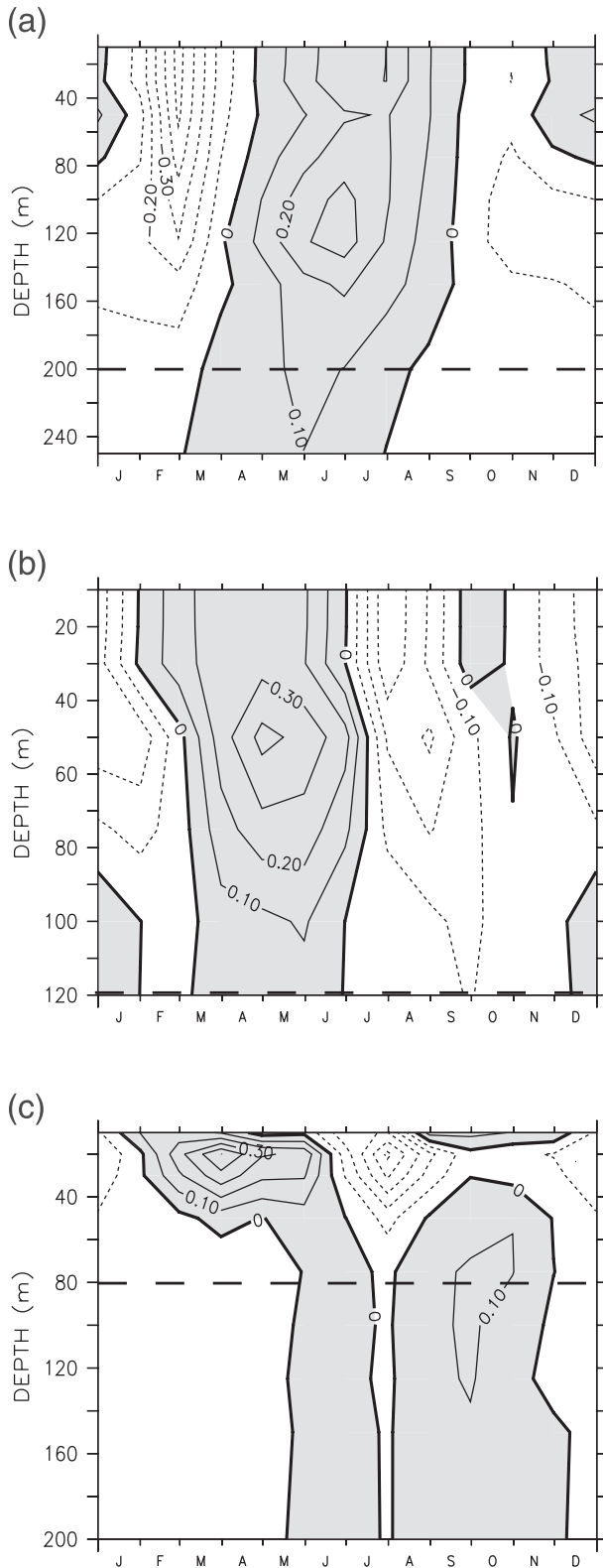


Figure 6. The vertical structure of the annual cycle of modeled zonal currents on the equator at 165°E, 140°W, and 110°W, plotted in terms of velocity anomalies (m s^{-1}). The dashed horizontal lines indicate the depths of the undercurrent. The model's annual cycle was generated using *Hellerman and Rosenstein [1983]* wind forcing. (Figure 6 may be directly compared with the observations presented in Figure 2.)

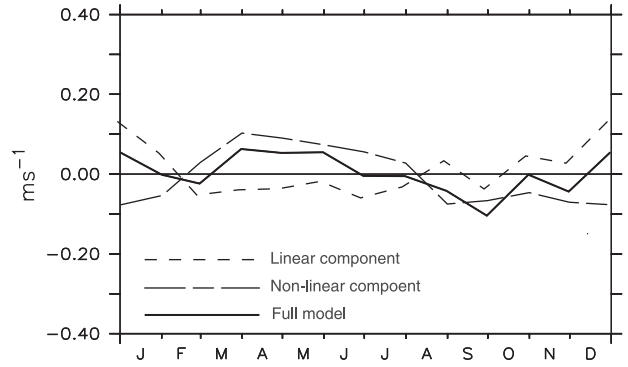


Figure 7. The annual cycle of modeled zonal currents in the EUC on the equator at 140°W and 120°m (solid curve), decomposed into contributions from the linear (short dashed curve) and nonlinear (long and short dashed curve) model components. Velocity anomalies are plotted in m s^{-1} . Comparison with Figure 3b clearly illustrates the inability of linear dynamics to model the annual cycle of the EUC and the accurate correcting behavior of the nonlinear component.

EUC) of the annual cycle of zonal currents, which shows that the STS is a feature of the Northern Hemisphere (Figure 8). At 140°W and 110°W a strong eastward surge in zonal currents that is centered at 2°N occurs at the time of

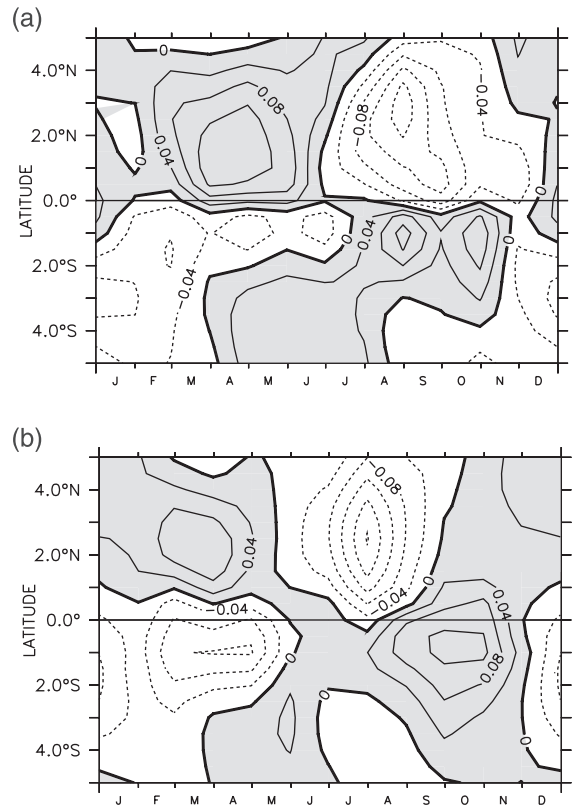


Figure 8. The meridional structure of the annual cycle of modeled zonal currents at the level of the EUC. (a) 140°W at 120 m and (b) 110°W at 80 m. Velocity anomalies are plotted in m s^{-1} . Note the strong surge in zonal currents north of the equator that occurs in the boreal spring; at 140°W the springtime surge in the EUC is clearly associated with the surge to the north.

the observed STS in EUC. Decomposition into linear and nonlinear components shows that all prominent features, including the off-equatorial STS, are due to linear dynamics; nonlinearity acts primarily as a meridional distortion of the linear features. In section 5.1 it will be demonstrated that the dominant nonlinear effect is mean meridional advection and that the modeled STS in the EUC at 140°W is due to this distortion. At 110°W the meridional distortion is significantly weaker, and there is no STS in the EUC. Consistently, though, there is a STS north of the equator. However, as discussed in section 5.3, the weakness of nonlinearity is likely due to both the model's weak equatorial cell at 110°W , which surface observations indicate to be less realistic, and inaccuracies in the wind field (which result in a poor simulation of the meridional structure of the annual cycle).

[32] In brief summary, linear dynamics are accurate in simulating the annual cycle of zonal currents at all three locations and at all levels, except in the EUC. Off the equator it would also seem that linear dynamics are dominant, even at the level of the EUC. In the EUC, nonlinearity is able to correct the linear annual cycle.

5. Analysis and Discussion

[33] The ability of linear dynamics to simulate the annual cycle of equatorial surface zonal currents and depth-integrated (surface to 200 m) zonal momentum has been covered by *Yu and McPhaden* [1999a, 1999b]. Here, taking advantage of the model's ability to accurately simulate the vertical structure of the annual cycle of zonal currents, we focus only on explaining the annual cycle of the EUC. Detailed analysis described here shows that mean meridional advection of the northern annual cycle of zonal currents is the dominant and driving nonlinearity, and that the dynamics of the antisymmetric annual cycle, which determines the annual cycle in the EUC, are easily understood in terms of equatorial wave dynamics.

5.1. Nonlinearity

[34] The annual cycle of nonlinear tendencies at 140°W in the EUC (Figure 9) identifies the terms responsible for producing the nonlinear component's correcting behavior. Local acceleration, $\partial u/\partial t$, is close to zero for most of the year, corresponding to periods of fairly constant nonlinear zonal velocity (i.e., the nonlinear component's velocity). Two periods of nonzero local acceleration, one in February and another in August, are responsible for sharp changes in nonlinear velocity and determine the character of the annual cycle. Meridional advection, $\partial v u/\partial y$, and vertical advection, $\partial w u/\partial z$, are by far the strongest terms. The annual cycle of meridional advection would explain the STS strongly peaking in May. Vertical advection counters the annual cycle of meridional advection, and in May, it cancels its effect almost alone. Together these two terms determine the structure of local acceleration and hence nonlinear zonal velocity. All other tendency terms are of similar magnitude and are fairly weak.

[35] The nonlinear component's appearance of simply extending the northern linear annual cycle to the equator

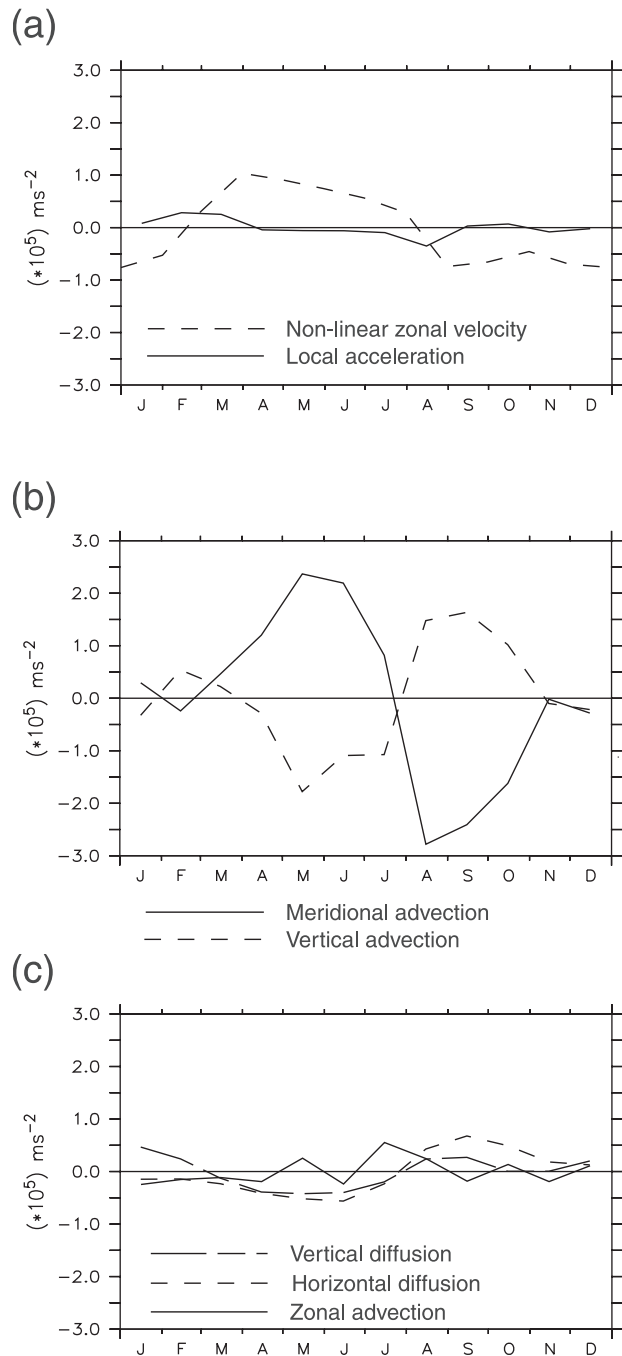


Figure 9. The annual cycle of the nonlinear component's tendency terms at 140°W , 0°N in the lower near-surface layer. (a) Local acceleration (solid curve) and the nonlinear component's zonal velocity anomaly (dashed curve and in m s^{-1}); (b) meridional advection (solid curve) and vertical advection (dashed curve); and (c) zonal advection (solid curve), horizontal diffusion (short dashed curve), and vertical diffusion (long and short dashed curve). The terms plotted are anomalies about the annual mean and in units of 10^{-5} m s^{-2} .

and the similarity in phase between meridional advection and northern zonal currents strongly suggests that mean meridional advection is important. To determine the role of the mean flow in determining nonlinearity, an anomaly

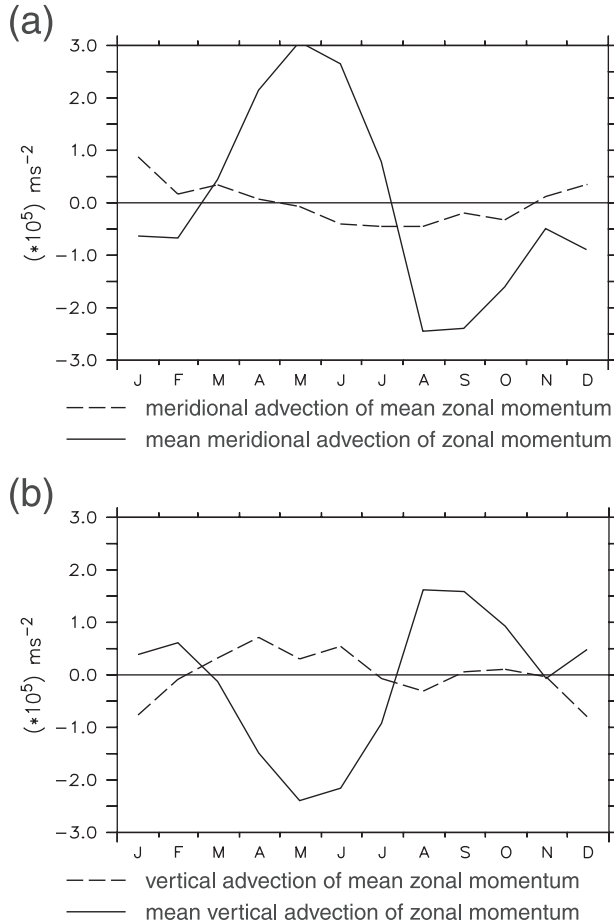


Figure 10. The annual cycle of the nonlinear component's advective tendency terms (shown in Figure 9b) are decomposed into anomaly terms. (a) Mean meridional advection of zonal momentum (solid curve) and meridional advection of mean zonal momentum (dashed curve). (b) Mean vertical advection of zonal momentum (solid curve) and vertical advection of mean zonal momentum (dashed curve). See the text for definitions. The terms plotted are anomalies about the annual mean and in units of 10^{-5} m s^{-2} .

form of the model was constructed. In the anomaly form the meridional advection and vertical advection terms are

$$\begin{aligned} \frac{\partial_{v'\bar{u}}}{\partial y} + \frac{\partial_{\bar{v}u'}}{\partial y} + \frac{\partial_{v'u'}}{\partial y}, \\ a \quad b \\ \frac{\partial_{w'\bar{u}}}{\partial z} + \frac{\partial_{\bar{w}u'}}{\partial z} + \frac{\partial_{w'u'}}{\partial z}, \\ c \quad d \end{aligned}$$

where terms with overbars and prime notations represent mean and anomaly quantities, respectively. The last terms in both equations (anomaly products) were found to be insignificant and are not discussed. Term a represents meridional advection of mean zonal momentum, b represents mean meridional advection of zonal momentum, c represents vertical advection of mean zonal momentum, and d represents mean vertical advection of zonal momentum.

These terms for the EUC at 140°W (Figure 10) show that the annual cycle of both meridional and vertical advection is primarily determined by advection of anomalous zonal velocity by the mean equatorial cell (i.e., terms b and d). Annual variations in the strength of the equatorial cell, terms a and c , are not significant. The effects of nonlinearity on the meridional structure are then easily interpreted as being due to mean meridional advection. Given the circulating direction of the equatorial cell, it is also clear that meridional advection is the driving term and that vertical advection is a reactive response; a surge in the EUC necessarily results in increased mean vertical advection (term d). The most likely reason that the annual cycle in the Northern Hemisphere dominates on the equator is that the annual variations in zonal currents are stronger in the north than in the south (Figure 8a). Another contributing factor is that the northern branch of the meridional cell is stronger than the southern branch (Figure 5c). However, observations [Qiao and Weisberg, 1997; Johnson et al., 2001] show that the reverse may hold, subject to much uncertainty with respect to aliasing.

5.2. Linearity and the Meridional Structure of the Annual Cycle

[36] Observations show that the meridional structure about the equator in the eastern equatorial Pacific of the annual cycle of surface zonal currents has a strong antisymmetric component [Reverdin et al., 1994]. The model matches surface observations closely and shows that this feature extends to the depth of the EUC, where through nonlinearity it explains the modeled STS in the EUC. The meridional structure of the annual cycle may be interpreted in terms of baroclinic modes, since it is determined by linear dynamics (section 4). The decomposition shows that the off-equatorial, antisymmetric component is only effectively owing to modes 1 and 2, and the equatorial symmetric component (particularly the incorrect January surge) is due to modes 6 and 7.

[37] Baroclinic modes 1 and 2 describe a balance among local acceleration, wind stress, and zonal pressure gradient that is primarily explained by the Kelvin and first Rossby waves of these baroclinic modes [Yu and McPhaden, 1999a, 1999b]. However, these waves are equatorially symmetric and hence do not explain the equatorially antisymmetric nature of the annual cycle. To determine which aspects of the linear dynamics and wind forcing are responsible for producing an equatorially antisymmetric response, a simple meridional mode model of these baroclinic modes was constructed (essentially that of Gill and Clarke [1974]). The model shows that the equatorially antisymmetric behavior is mainly due to the second meridional Rossby wave, with significant contributions from both baroclinic modes (see Figure 11, to be compared with Figure 8).

[38] The second meridional mode Rossby wave is forced by equatorially antisymmetric variations in zonal wind stress [see Gill, 1982], which for the first and second baroclinic modes are between 10°S and 10°N . (Although meridional winds strongly influence the mean meridional circulation in the eastern equatorial Pacific, our results show that they do not contribute significantly to the annual cycle of linear zonal currents within a few degrees of the equator.) Seasonal variations in zonal winds between these latitudes

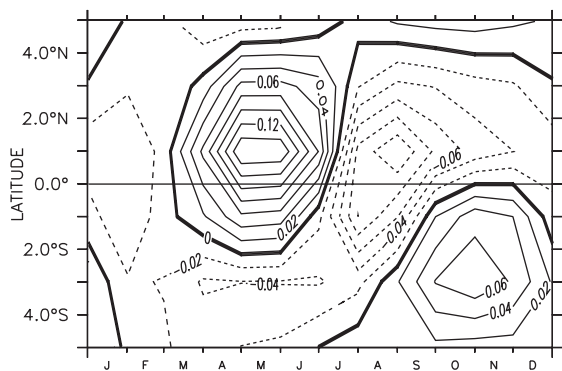


Figure 11. The meridional structure of the annual cycle of zonal currents at 140°W , 120 m (the depth of the EUC) generated by a meridional mode model [Gill and Clarke, 1974]. The model consists of the first two baroclinic modes and their Kelvin and first and second Rossby waves. The model covers the equatorial Pacific (125°E – 89°W by 29°S – 29°N), was forced with observed zonal winds [Hellerman and Rosenstein, 1983] using spatially constant wind projection coefficients (basin averages of those used in our main model), and includes eastern and western boundary reflections. Meridional winds were neglected, since they do not contribute significantly to the linear annual cycle. Velocity anomalies are plotted in m s^{-1} with a contour interval of 0.02 m s^{-1} .

have a strong equatorially antisymmetric component, since the trade winds are strongest in the winter hemisphere. Thus the second meridional Rossby wave extends the balance among zonal pressure gradient, local acceleration, and wind stress on the equator off the equator.

[39] Baroclinic modes 6 and 7 are locally forced, since they have short damping scales, 17° and 9° , respectively. The surface zonal currents associated with these modes are positively correlated to zonal wind forcing directly to the west. In the EUC the correlation becomes negative owing to the vertical structure of these modes. The linear model's behavior is as expected; the EUC is strongest (weakest) when the equatorial trades are strongest (weakest). Interestingly, elsewhere these modes behave appropriately: They almost solely determine the magnitude and vertical and zonal structure of the EUC and contribute significantly to the annual cycle of zonal currents at 165°E . This inconsistency suggests that the linear component's failure in simulating the annual cycle of the EUC is due to the breakdown of linear assumptions rather than the use of a modal solution or poor choice of parameters. Sensitivity studies support this assertion (Appendix A).

5.3. Difficulties Simulating Nonlinearity

[40] At 110°W the model is unable to simulate the annual cycle in the EUC. Consistent with the picture at 140°W , linear dynamics show a STS north of the equator and incorrect behavior in the EUC (Figure 8b). Here, though, the nonlinear correction is weak over the whole year. Analysis shows that mean meridional advection is weak; hence the off-equatorial structure is unable to influence the annual cycle on the equator, and the mechanism described in section 5.1 is not active. Mean meridional advection at

110°W is weak for two reasons. First, the model's meridional circulation is much weaker here than at 140°W ; second, the meridional structure of the annual cycle is also weaker here.

[41] Lack of observations makes it difficult to assess the model's equatorial cell at 110°W . A comparison with Reverdin *et al.*'s [1994] 15 m current climatology shows that the northern surface branch of the equatorial cell between the equator and 2°N , east of 140°W , is unrealistically strong. This would indicate that the equatorial cell is less well modeled at 110°W than at 140°W . However, the surface observations may be biased, because the only time drifters spend a significant time near the equator is during El Niños. Nonetheless, meridional currents were found to depend crucially on the higher-order baroclinic modes which, because they are strongly damped, are sensitive to both the precise spatial pattern of wind stress and the vertical mixing formulation. The latter is consistent with other work [World Climate Research Programme, 1995]. The less-than-perfect representation in the model of the equatorial cell, therefore, is likely a result of both inaccurate wind stress forcing and crude vertical mixing.

[42] Lack of observations at the depth of the EUC also makes it difficult to assess the model's simulation of the meridional structure of the annual cycle about the EUC. However, the meridional structure of the annual cycle of zonal currents is highly sensitive to the representation of wind stress (Appendix A) and thus may not be accurately represented either. The clear-modeled STS north of the equator suggests that the inability to model the annual cycle in the EUC at 110°W is due to poor modeling of both the equatorial cell and the meridional structure of the annual cycle rather than to a different mechanism.

[43] The incorrect response of nonlinearity at the surface and in the western Pacific must also be addressed. In these regions the linear model is able to accurately reproduce the annual cycle, suggesting that either the nonlinear terms are negligible in these regions on the annual timescale or that they balance each other on the annual timescale. Neither of these situations occur in the mean. As the addition of nonlinearity effects the model's simulation of the annual cycle, it would appear that nonlinearity is not negligible. The second idea agrees with Wacongne [1989], who analyzed the zonal momentum balance of the equatorial Atlantic using the Philander and Pacanowski [1984] model. In the annual cycle the following balance was found:

$$vu_y + wu_z = -\frac{P_x}{\rho_0} + (vu_z)_z,$$

with all four terms varying in strength seasonally but their sum remaining fairly constant. Note that local acceleration is absent. Given the crudeness of our model and the importance in our model of representing the mean equatorial cell correctly, it is not surprising that the model is unable to resolve this fine balance.

6. Summary

[44] The annual cycle of the EUC is characterized by an eastward surge in currents occurring in the boreal spring, a time when the surface trade winds are weak. Zonal currents above the EUC, in a direct response to the weakened winds,

also surge eastward at this time [Yu and McPhaden, 1999a, 1999b]. Modeling [Wacongne, 1989] and observational studies [Johnson and Luther, 1994; Peters et al., 1988; Qiao and Weisberg, 1997] indicate that wind stress is not significant in the momentum balance of the EUC. Hence the STS in the undercurrent is not so easily understood.

[45] Using a simple model which separates linear and nonlinear effects, a mechanism for the annual cycle of the EUC is presented. North of the equator, the annual cycle of zonal currents surges in spring at the surface and at the depth of the undercurrent. The springtime surge in the EUC is the result of mean advection by the meridional circulation of the northern annual cycle onto the equator. The ability of mean meridional advection to advect the northern annual cycle onto the equator is demonstrated.

[46] The meridional structure of the annual cycle of zonal currents in the model (and in surface observations) from the surface to the EUC has a strong equatorially antisymmetric component. This is a response to annual variations in the trade winds, which are antisymmetric about the equator and can be understood in terms of linear wave dynamics. The balance among zonal pressure gradient, wind stress, and local acceleration that holds on the equator [Yu and McPhaden, 1999a] also holds off the equator. The second meridional Rossby wave is responsible for extending this balance off the equator to produce the antisymmetric response.

[47] The simple mechanism presented here does not take into account variations in the mass field. Nor is the model, because of its simplicity, able to accurately model aspects of the meridional circulation. However, the model's simplicity is an advantage when dealing with the complex dynamics of equatorial currents, and it is this simplicity that allowed the interpretation of the annual cycle presented here. The model also shows promising results in the simulation of interannual variability of surface zonal currents and SST (when coupled to a simple SST model). These results will be discussed elsewhere.

Appendix A: Model Equations

[48] The model represents the sum of two components, which were defined in section 3 and referred to as linear and nonlinear. The model's linear component is a modal solution to the equations in (1), consisting of 10 baroclinic modes plus two surface layers modeling modes 11–30; and the nonlinear is a two-layer solution of the highly simplified residual nonlinear momentum equations in (2). Here these three components are defined explicitly, with some brief details on their derivation.

[49] The baroclinic model is given by

$$u = \sum_{n=1}^{10} u_n \psi_n, \quad v = \sum_{n=1}^{10} v_n \psi_n, \quad \rho = \sum_{n=1}^{10} \rho_n \psi_n$$

$$w = \sum_{n=1}^{10} w_n \int_{-H}^z \psi_n dz, \quad \rho = \sum_{n=1}^{10} \rho_n \psi_{nz}, \quad (\text{A1})$$

where the baroclinic modes are defined by the following vertical structure equation:

$$(N^{-2} \psi_{nz})_z = -c_n'^{-2} \psi_n, \quad (\text{A2})$$

and satisfying upper and lower boundary conditions

$$N^{-2} \psi_{nz} + g^{-1} \psi_n = 0; \quad z = 0$$

$$\psi_{nz} = 0; \quad z = -H. \quad (\text{A3})$$

The equation governing the expansion coefficients are

$$u_{nt} + r_n u_n - f v_n + p_{nx} = \tau_n^x + \nu_h \nabla_h^2 u_n,$$

$$v_{nt} + r_n v_n + f u_n + p_{ny} = \tau_n^y + \nu_h \nabla_h^2 v_n,$$

$$c_n'^{-2} (p_{nt} + r_n p_n + \nu_h \nabla_h^2 p_n) + u_{nx} + v_{ny} = 0,$$

$$w_n = c_n'^{-2} (p_{nt} + r_n p_n + \nu_h \nabla_h^2 p_n),$$

$$\rho_n = -g^{-1} p_n, \quad (\text{A4})$$

where

$$r_n = \frac{A}{c_n'^2}, \quad \tau_n^x = \frac{\tau^x \psi_n(0)}{D_n}, \quad \tau_n^y = \frac{\tau^y \psi_n(0)}{D_n}, \quad (\text{A5})$$

and $D_n = \int_{-H}^0 \psi_n^2 dz$. In the solution above, N^2 , ψ_n , and c_n' vary horizontally, but c_n is taken as a constant. The equations in (A4) are easily derived by substituting the equations in (A1) into the equations in (1), using mode orthogonality and neglecting mode mixing (terms arising from horizontal varying modes). The barotropic mode is also neglected.

[50] The model also calculates horizontal velocity in two surface layers and vertical velocity at the layer interface due to modes 11–30. The governing equations (A6) are obtained consistently from the full modal solutions. The simplified Ekman form derives from the fact that owing to strong mode damping, local acceleration and horizontal diffusion are negligible. Pressure and density variations are also neglected, since the vertical structure of high-order modes means they contribute little to the full fields.

$$\underline{\mathbf{u}}_{H_1} = \frac{1}{\Delta H_1} \underline{\mathbf{A}}_{H_1} \cdot \underline{\boldsymbol{\tau}},$$

$$\underline{\mathbf{u}}_{H_2} = \frac{1}{\Delta H_2} \underline{\mathbf{A}}_{H_2} \cdot \underline{\boldsymbol{\tau}}, \quad (\text{A6})$$

$$w_{H_1} = \nabla \cdot \left(\underline{\mathbf{A}}_{H_1} \cdot \underline{\boldsymbol{\tau}} \right),$$

where $\underline{\mathbf{u}} = (u, v)$ is the horizontal velocity within a layer; subscripts H_1 and H_2 denote upper and lower layers, respectively; $\Delta H_1 = H_1$ and $\Delta H_2 = H_1 - H_2$ are the thickness of the upper and lower layers, respectively; and $\underline{\boldsymbol{\tau}} = \begin{pmatrix} \tau_x \\ \tau_y \end{pmatrix}$ is the vector wind stress. The variable w_{H_1} is the vertical velocity at the base of the upper layer and is the vertical integral of the divergence of flow in the upper layer with vertical velocity vanishing at the surface. Matrices $\underline{\mathbf{A}}_{H_1}$ and $\underline{\mathbf{A}}_{H_2}$ are given by

$$\underline{\mathbf{A}}_{H_1} = \sum_{n=11}^{30} \frac{\psi_n(0)}{D_n} \int_{-H_1}^0 \psi_n(z) dz \underline{\mathbf{A}}_n,$$

$$\underline{\mathbf{A}}_{H_2} = \sum_{n=11}^{30} \frac{\psi_n(0)}{D_n} \int_{-H_2}^{H_1} \psi_n(z) dz \underline{\mathbf{A}}_n. \quad (\text{A7})$$

They represent the sum of the individual contributions of modes 11–30. The separation into vertical modes permits the straightforward integration across the layers. Matrix $\underline{\underline{A}}_n$, given by

$$\underline{\underline{A}}_n = \frac{1}{(r_n^2 + f^2)} \begin{pmatrix} r_n & f \\ -f & r_n \end{pmatrix},$$

represents the horizontal component of mode n 's contribution to the flow. $\underline{\underline{A}}_n \cdot \underline{\underline{\tau}}$ is the solution of Ekman equations that are obtained from equation (A4).

[51] The nonlinear component of the model is obtained via vertical integration of the equations in (2) over the two layers, which gives

$$\begin{aligned} \frac{\partial}{\partial t} (\Delta H_1 u_{H_1}^{nl}) &= -\frac{\partial}{\partial x} (\Delta H_1 u_{H_1} u_{H_1}) - \frac{\partial}{\partial y} (\Delta H_1 u_{H_1} v_{H_1}) \\ &\quad - [u_{H_1} w M(w) + u_{H_2} w M(-w)] \\ &\quad + \nu_h \nabla_h \cdot \Delta H_1 \nabla_h u_{H_1}^{nl} + \nu_v \left(\frac{u_{H_2}^{nl} - u_{H_1}^{nl}}{\Delta H_1 + \Delta H_2} \right), \\ \frac{\partial}{\partial t} (\Delta H_2 u_{H_2}^{nl}) &= -\frac{\partial}{\partial x} (\Delta H_2 u_{H_2} u_{H_2}) - \frac{\partial}{\partial y} (\Delta H_2 u_{H_2} v_{H_2}) \\ &\quad + [u_{H_1} w M(w) + u_{H_2} w M(-w)] \\ &\quad + \nu_h \nabla_h \cdot \Delta H_2 \nabla_h u_{H_2}^{nl} + \nu_v \left(\frac{u_{H_1}^{nl} - u_{H_2}^{nl}}{\Delta H_1 + \Delta H_2} \right), \\ w^{nl} &= -\frac{\partial}{\partial x} (\Delta H_1 u_{H_2}^{nl}), \end{aligned} \quad (\text{A8})$$

where superscripts nl and l denote terms from the nonlinear and linear components, respectively; subscripts are as in equation (A6); and u and w are the model's full zonal velocity and vertical velocity at the layer interface, respectively. $M()$ is the Heaviside function.

Appendix B: Sensitivity Studies

[52] This appendix presents a brief summary of the extensive sensitivity studies that were performed to determine the robustness of the results presented in section 4. These experiments support the model findings by demonstrating that the model parameters and layers are appropriate, the modal solution is consistent, and the important features of the mechanism are not wind field unique.

B.1. Diffusion Parameters

[53] The model was tested to a wide range of vertical diffusion parameter values, $0.5-6(\times 10^{-7}) \text{ m}^2 \text{ s}^{-3}$. In agreement with other authors [Minobe and Takeuchi, 1995; Yu and McPhaden, 1999a] the vertical diffusion parameter affects the strength of the solution: Increased damping leading to weaker zonal currents and vice versa. This parameter is given a wide range of values ($1.4 \times 10^{-7} \text{ m}^2 \text{ s}^{-3}$ [Minobe and Takeuchi, 1995] to $6 \times 10^{-7} \text{ m}^2 \text{ s}^{-3}$ [Yu and McPhaden, 1999a]); the choice appears to be related to the wind product used. Our experiments clearly showed that the model's parameter value is appropriate and, in addition, that the annual cycle of the EUC remains unchanged within the parameter range where the EUC is defined.

[54] The model's sensitivity to the parameterization of vertical diffusion was also tested through independently specifying mode damping (as opposed to being inversely proportional to the square of the shallow water speeds). The model was also tested to decreased and increased values of horizontal diffusion ($\nu_h = 1. \times 10^2 \text{ m}^2 \text{ s}^{-1}$ and $3.5 \times 10^2 \text{ m}^2 \text{ s}^{-1}$) and to higher and lower values of the nonlinear component's vertical diffusion coefficient ($\nu_v = 1. \times 10^{-2}$ and $1. \times 10^{-4} \text{ m}^2 \text{ s}^{-1}$). While these changes of course affected the simulations, the annual cycle of the EUC remained a robust feature.

B.2. Model Layers

[55] To test the sensitivity of the results to the specification of the two surface layers, a variety of different configurations were implemented, in which the thickness and positions of the layers were altered. These included constant thickness layers, arbitrarily increasing and decreasing the depth of the upper layer, and changing the lower boundary of the lower layer to give lower layers of constant thickness. In all cases neither the mean currents nor the annual cycle exhibited any significant sensitivity, demonstrating that the two layers are adequate in capturing the basic effects of the neglected processes and that the model's simulation is not highly sensitive to their specification.

B.3. Mode Mixing

[56] As stated earlier, scattering of modes due to horizontal variations in stratification (mode mixing) is neglected, although it cannot be justified with scale arguments. To assess the neglect of mode mixing, we performed a number of numerical experiments using a finite difference model of the equations in (1), as opposed to a modal solution (The eddy coefficients for vertical diffusion of heat and momentum were taken to be inversely proportional to the square of Brunt-Väisälä frequency, as in the modal model.) The model corresponded closely to the modal solution, producing similar results when forced with climatological winds, and in particular the annual cycle of the EUC remained incorrect.

[57] The experiments to measure mode mixing consisted of comparing the propagation of Kelvin wave pulses from the dateline to the eastern Pacific through horizontally constant and horizontally varying stratifications. The horizontally varying stratification was that used to calculate the baroclinic modes, and the horizontally constant stratification was taken from 180°E , 0°N . Seven different Kelvin waves, corresponding closely to the first seven baroclinic modes, were tested. Zonally, the Kelvin waves consisted of a 20° sinusoid hump centered on the dateline. In all cases, horizontal variations in stratification were found to slow the propagation of the waves and alter their vertical structure but not to cause significant mode mixing. The most interesting result was that stratification modified the vertical structure of the modes to match those of the background stratification, strongly supporting our use of horizontally varying baroclinic modes. Mode mixing among higher-order modes is not a significant issue here. These modes are strongly damped and so do not contribute significantly to the adjustment process.

B.4. Wind Forcing

[58] The sensitivity of the results to different wind forcing was tested by using a climatology created primarily from the Florida State University (FSU) [Stricherz *et al.*, 1997] winds over the period 1979–1998. (NCEP reanalysis [Kalnay *et al.*, 1996] winds were used over the Atlantic and at high latitudes not covered by FSU winds.) The zonal, meridional, and vertical structure of the mean currents did not differ significantly from that generated using Helleman and Rosenstein [1983] wind stress, but the magnitude of the currents was up to 20% weaker. Such differences have been reported [Yu and McPhaden, 1999a]. While the annual cycle along the equator is also noticeably weaker, the westward phase propagation and vertical structure of the annual cycle were similar. Significant differences occurred in the meridional structure of the annual cycle at the depth of the EUC: While the same off-equatorial features important to the annual cycle of the EUC described in section 5 are present, they are much weaker. As a consequence, the meridional distortion of nonlinearity is not so apparent, and its effect on the annual cycle of EUC is weaker. This clearly suggests that correct representation of zonal wind stress is important to modeling the annual cycle of the EUC.

[59] **Acknowledgments.** This work was supported by the Australian Government Cooperative Research Centre program and the Australian Bureau of Meteorology. We also thank the TAO Project Office for providing current data.

References

- Cai, W., and P. H. Whetton, Evidence for time-varying pattern of greenhouse warming in the Pacific ocean, *Geophys. Res. Lett.*, *27*, 2577–2580, 2000.
- Cane, M., Modeling sea level during El Niño, *J. Phys. Oceanogr.*, *14*, 1864–1874, 1984.
- Dewitte, B., G. Reverdin, and C. Maes, Vertical structure of an OGCM simulation of the equatorial Pacific ocean in 1985–94, *J. Phys. Oceanogr.*, *29*, 1542–1570, 1999.
- Gill, A. E., *Atmosphere-Ocean Dynamics*, Academic, San Diego, Calif., 1982.
- Gill, A. E., and A. J. Clarke, Wind-induced upwelling, coastal currents, and sea-level changes, *Deep-Sea Res.*, *21*, 325–345, 1974.
- Gu, D., and S. G. H. Philander, Interdecadal climate fluctuations that depend on exchanges between the tropics and the extratropics, *Science*, *275*, 805–807, 1997.
- Harrison, D. E., On climatological monthly mean wind stress and wind stress curl fields over the world ocean, *J. Clim.*, *2*, 57–70, 1989.
- Helleman, S., and M. Rosenstein, Normal monthly wind stress over the world ocean with error estimates, *J. Phys. Oceanogr.*, *13*, 1093–1104, 1983.
- Johnson, E. S., and D. S. Luther, Mean zonal momentum balance in the upper and central equatorial Pacific ocean, *J. Geophys. Res.*, *99*, 7689–7705, 1994.
- Johnson, E. S., and M. J. McPhaden, Interior pycnocline flow from the subtropical to the equatorial Pacific ocean, *J. Phys. Oceanogr.*, *29*, 3073–3089, 1999.
- Johnson, E. S., M. J. McPhaden, and E. Firing, Equatorial Pacific ocean horizontal velocity, divergence, and upwelling, *J. Phys. Oceanogr.*, *31*, 839–849, 2001.
- Kalnay, E., et al., The NCEP/NCAR 40-year Reanalysis Project, *Bull. Am. Meteorol. Soc.*, *77*, 437–471, 1996.
- Levitus, S., Climatological atlas of the world ocean, *Prof. Pap.* *13*, 173 pp., Natl. Ocean. and Atmos. Admin., Silver Spring, Md., 1982.
- McCreary, J. P., A linear stratified ocean model of the equatorial undercurrent, *Philos. Trans. R. Soc. London, Ser. A*, *298*, 603–635, 1981.
- McCreary, J. P., and P. Lu, On the interaction between the subtropical and equatorial ocean circulation: Subtropical cell, *J. Phys. Oceanogr.*, *24*, 466–497, 1994.
- Minobe, S., and K. Takeuchi, Annual period equatorial waves in the Pacific ocean, *J. Geophys. Res.*, *100*, 18,379–18,392, 1995.
- Peters, H., M. C. Gregg, and J. M. Toole, On the parameterization of equatorial turbulence, *J. Geophys. Res.*, *93*, 1199–1218, 1988.
- Philander, S. G., *El Niño, La Niña, and the Southern Oscillation*, Academic, San Diego, Calif., 1990.
- Philander, S. G. H., and R. C. Pacanowski, Simulation of the seasonal cycle in the tropical Atlantic ocean, *Geophys. Res. Lett.*, *11*, 802–804, 1984.
- Qiao, L., and R. H. Weisberg, The zonal momentum balance of the equatorial undercurrent in the central Pacific, *J. Phys. Oceanogr.*, *27*, 1094–1119, 1997.
- Reverdin, G., C. Frankignoul, E. Kestenare, and M. J. McPhaden, Seasonal variability in the surface currents of the equatorial Pacific, *J. Geophys. Res.*, *99*, 20,323–20,344, 1994.
- Stricherz, J. N., D. M. Legler, and J. J. O'Brien, *TOGA Pseudo-stress Atlas 1985–1994*, vol. 2, Pacific Ocean, 158 pp., Florida State Univ., Tallahassee, 1997.
- Wacongne, S., Dynamical regimes of a fully nonlinear stratified model of the Atlantic equatorial undercurrent, *J. Geophys. Res.*, *94*, 4801–4815, 1989.
- World Climate Research Programme, Comparison of TOGA tropical Pacific Ocean model simulations with the WOCE/TOGA surface velocity programme, *Rep. 4/1995*, 156 pp., TOGA Numer. Exp. Group, Scripps Inst. of Ocean., La Jolla, Calif., 1995.
- Yu, X., and M. J. McPhaden, Seasonal variability in the equatorial Pacific, *J. Phys. Oceanogr.*, *29*, 925–947, 1999a.
- Yu, X., and M. J. McPhaden, Dynamical analysis of seasonal and inter-annual variability in the equatorial Pacific, *J. Phys. Oceanogr.*, *29*, 2350–2369, 1999b.
- Yu, Z., P. S. Schopf, and J. P. McCreary, On the annual cycle of upper-ocean circulation in the eastern equatorial Pacific, *J. Phys. Oceanogr.*, *27*, 309–324, 1997.
- Yu, Z., J. P. McCreary, W. S. Kessler, and K. A. Kelly, Influence of equatorial dynamics on the Pacific North Equatorial Countercurrent, *J. Phys. Oceanogr.*, *30*, 3179–3190, 2000.

N. Keenlyside, Max Planck Institute for Meteorology, Bundesstr 55, 20146 Hamburg, Germany. (keenlyside@dkrz.de)
 R. Kleeman, 251 Mercer Street, New York, NY 10012, USA. (kleeman@cims.nyu.edu)